Computers, Materials & Continua

Tech Science Press

Doi:10.32604/cmc.2025.058495

ARTICLE

Local Content-Aware Enhancement for Low-Light Images with Non-Uniform Illumination

Qi Mu*, Yuanjie Guo, Xiangfu Ge, Xinyue Wang and Zhanli Li

College of Computer Science and Technology, Xi'an University of Science and Technology, Xi'an, 710054, China

*Corresponding Author: Qi Mu. Email: muqi@xust.edu.cn

Received: 13 September 2024; Accepted: 17 December 2024; Published: 06 March 2025

ABSTRACT: In low-light image enhancement, prevailing Retinex-based methods often struggle with precise illumination estimation and brightness modulation. This can result in issues such as halo artifacts, blurred edges, and diminished details in bright regions, particularly under non-uniform illumination conditions. We propose an innovative approach that refines low-light images by leveraging an in-depth awareness of local content within the image. By introducing multi-scale effective guided filtering, our method surpasses the limitations of traditional isotropic filters, such as Gaussian filters, in handling non-uniform illumination. It dynamically adjusts regularization parameters in response to local image characteristics and significantly integrates edge perception across different scales. This balanced approach achieves a harmonious blend of smoothing and detail preservation, enabling more accurate illumination estimation. Additionally, we have designed an adaptive gamma correction function that dynamically adjusts the brightness value based on local pixel intensity, further balancing enhancement effects across different brightness levels in the image. Experimental results demonstrate the effectiveness of our proposed method for non-uniform illumination images across various scenarios. It exhibits superior quality and objective evaluation scores compared to existing methods. Our method effectively addresses potential issues that existing methods encounter when processing non-uniform illumination images, producing enhanced images with precise details and natural, vivid colors.

KEYWORDS: Retinex; non-uniform low illumination; local content-aware; effective guided image filtering

1 Introduction

Images contain rich information and are indispensable to a wide array of high-level computer vision tasks. Nonetheless, their quality can be compromised under low-light conditions, typically exhibiting diminished contrast, reduced brightness, and obscured details. These degradations challenge human visual perception and impede the accuracy of critical computer vision tasks, such as object detection, tracking, and semantic segmentation. Thus, developing effective low-light image enhancement techniques has become a prominent research focus [1,2].

Retinex-based [3] methods have distinguished themselves by achieving a dynamic balance across multiple aspects, particularly excelling in color retention and detail enhancement in low-light conditions [4–6]. These methods employ filters as center-surround functions to estimate illumination and subsequently mitigate its effects. The accuracy of this estimation relies on the performance of the filters. Traditional Retinex methods, utilizing isotropic filters, have successfully increased the brightness of low-light images and unveiled details in dark regions. However, when applied to non-uniformly illuminated images, these isotropic filters are prone to deviations at illumination transition regions, resulting in halo artifacts and detail

loss, as exemplified by the multi-scale Retinex with color restoration (MSRCR) [7] method in Fig. 1b. To overcome these limitations, researchers have developed novel Retinex enhancement methods, categorized into traditional and deep learning strategies.

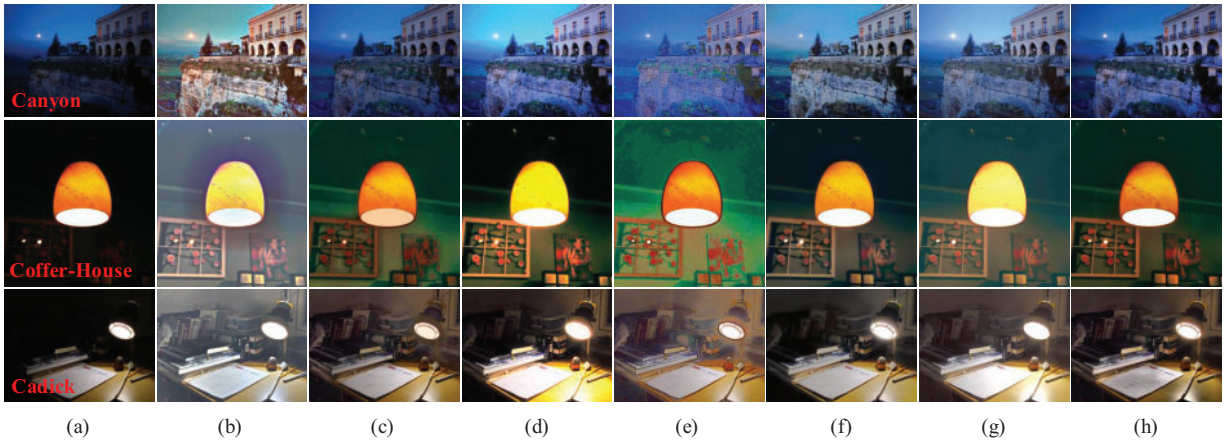

Figure 1: The enhanced results of different methods in images with non-uniform low illumination: (a) Original images, (b) MSRCR, (c) NPE, (d) Mu's method, (e) Retinex-Net, (f) KinD, (g) URetinex-Net, (h) Ours

In traditional Retinex enhancement methods, a series of anisotropic filters has been implemented to estimate illumination [8]. Although these methods offer some relief from halo artifacts and improve the natural rendering of colors, they still encounter difficulties with accurately estimating illumination at areas of light transition. This limitation can result in edge blur in the enhanced images, as exemplified by the naturalness preserved enhancement (NPE) [9] method shown in Fig. 1c. Additionally, these methods may not constantly adjust brightness finely across different regions of an image, potentially resulting in inadequate enhancement of dark areas or over-enhancement of the bright areas, as illustrated by the Mu et al. [10] in Fig. 1d.

In recent years, advances in deep neural networks have prompted researchers to utilize these sophisticated models to separate and adjust illumination and reflectance components in images. Compared to traditional methods, deep learning approaches have demonstrated superior brightness enhancement capabilities and a reduced propensity for halo artifacts at illumination transitions, as illustrated by models such as deep Retinex network (Retinex-Net) [11], Kindling the Darkness network (KinD) [12], and Retinex-based deep unfolding network (URetinex-Net) [13]. Nonetheless, the absence of an optimized network structure can sometimes result in the loss of features during the decomposition process, potentially leading to blurred details, as shown in Fig. 1e,f. The performance of supervised learning-based low-light image enhancement methods solutions largely depends on the training dataset, including its size, diversity, and differences from real-world data, all of which can impact the model's performance [14]. As a result, some deep learning methods may risk over-enhancing bright regions when dealing with non-uniformly illuminated images, as shown in Fig. 1g.

To cope with the above problems, we propose a novel local content-aware enhancement method for low-light images with non-uniform illumination. Our approach effectively mitigates halo artifacts, edge blurring, and over-enhancement in bright regions while simultaneously removing noise and preserving essential image details, as illustrated in Fig. 1. Our contributions are as follows:

(1) We proposed a multi-scale effective guided filtering approach complemented by an adaptive gamma correction function. This integrated methodology ensures precise illumination estimation and adjustment across diverse image regions, tailored to the specific characteristics of each local area within the image.
(2) We utilized an effective guided filter to denoise the reflectance component, focusing on edge preservation and accurate noise removal. Subsequently, we implemented a detail enhancement process on the denoised image, preventing noise amplification during the enhancement process.
(3) We conducted comprehensive experiments on six varied low-light image datasets encompassing a range of scenes. Our method was rigorously compared with several mainstream Retinex enhancement methods. These experiments substantiated the effectiveness of our approach in enhancing low-light images, particularly under non-uniform illumination conditions.

2 Related Work

2.1 Image Enhancement through Gray Mapping Techniques

Gray mapping methods adjust brightness and contrast by compressing or stretching pixel values point-by-point. Representative methods include gamma correction and histogram equalization (HE). Gamma correction adjusts brightness using a nonlinear transformation. Global correction parameters struggle with non-uniform illumination. Hence, adaptive gamma correction functions have been developed [15]. Histogram equalization enhances contrast by expanding the dynamic range of pixel values. Early global methods processed all pixels uniformly, ignoring local differences. This often led to over-enhancement and noise amplification in low-light images with non-uniform illumination. Consequently, many local HE methods and improvements have been proposed to enhance brightness and contrast [16,17].

Gray mapping methods ignore the influence of spatial context, making the image prone to over-enhancement and detail loss, which results in an unnatural appearance. They are typically used with other methods to improve enhancement effects in practical applications [8,18].

2.2 Retinex-Based Image Enhancement

Land proposed the Retinex theory [3] based on color constancy. This theory effectively models color perception in the human visual system. According to the Retinex theory, the image P can be decomposed into two components: the reflectance component R and the illumination component I. The mathematical description is given in Eq. (1).

$$P = I \cdot R \tag{1}$$

The core of Retinex-based image enhancement methods is to remove or suppress the influence of the illumination component from the original image P. The key lies in accurately estimating the illumination. Early Retinex enhancement methods assumed uniform illumination, using isotropic Gaussian filtering (GF) for estimation and treating the reflectance component as a result. However, real-world illumination is non-uniform, and GF often fails at light transition areas, leading to halo artifacts, edge blurring, and detail loss in enhanced images. To address these issues, anisotropic bilateral filtering (BF) [19] has been applied for illumination estimation, enhancing image details, and reducing halo phenomena. However, gradient reversal near edges causes artifacts. The NPE method combines neighborhood brightness information with a bright-pass filter and dual-logarithm transformation to enhance detail and naturalness. Many researchers use guided image filters (GIF) [20] and their improved versions for more accurate illumination estimation [21]. Unlike these, Fu et al. [22] designed a weighted variational model for better prior modeling and edge

preservation. The structure-revealing low-light image enhancement (SRLIE) [23] method introduces various priors to construct an optimization function, effectively suppressing noise and halo phenomena.

Deep learning-based low-light image enhancement methods have made significant progress recently. Zhang et al. proposed KinD, which reduces noise and preserves color fidelity by training on paired datasets under different exposure conditions. However, the enhanced images still exhibit light spots and blurred details in some cases. To address these issues, Zhang et al. [24] introduced an improved version, KinD++, which incorporates a multi-scale illumination attention module to significantly reduce light spots and detail blurring. Nevertheless, when processing images with non-uniform illumination, artifacts may still appear in areas with abrupt lighting transitions. Wu et al. [13] introduced URetinex-Net, a deep unfolding network that effectively restores clear details while suppressing noise, though it tends to over-enhance non-uniformly illuminated images. Cai et al. [25] presented Retinexformer, the first Transformer method with Retinex theory, which improves low-visibility areas, removes noise, and avoids artifacts. Compared to traditional methods, deep learning approaches recover details and restore colors more accurately by learning rich features and contextual information, enhancing visual quality. However, they require large annotated datasets, complex training, and high computational resources.

2.3 Guided Filter-Based Illumination Estimation

The GIF is an anisotropic filter that establishes a local linear relationship between the guide image G and the filtered result image O, as shown in Eq. (2).

$$O_i = a_k G_i + b_k, \forall i \in \omega_k \tag{2}$$

where i denotes the pixel coordinates in the image, ω_k denotes the square neighborhood window centered at pixel k, and (a_k, b_k) denotes the coefficients of the linear constant term within the neighborhood window.

The values of (a_k, b_k) are obtained by establishing the cost function $E(a_k, b_k)$ (as shown in Eq. (3)) between the filtered result image and the image to be enhanced.

$$E(a_k, b_k) = \sum_{i \in \omega_k} (a_k \mathrm{G}_i + b_k - X_i)^2 + \varepsilon a_k^2 \tag{3}$$

where X_i represents the image to be processed, and $\boldsymbol{\varepsilon}$ is the regularization parameter, which acts as a penalty coefficient to prevent a_k from becoming too large and determines the filtering effect.

GIF uses the guide image's structural information to adjust weights. GIF ensures that the output image shares the same gradient edges as the guide image, effectively avoiding the gradient reversal problem in BF [26]. However, GIF uses the same regularization parameter in all filtering windows, overlooking regional differences in non-uniform illumination. This results in halo artifacts and edge blurring in areas with significant texture variations. To address this, researchers have developed improved versions of GIF for illumination estimation. Weighted guided image filtering (WGIF) [27] introduces edge-aware weights and adaptively adjusts the regularization factor, better preserving edges and preventing blurring. Gradient domain guided image filtering (GGIF) [28] further enhances filtering performance by incorporating multi-scale edge-aware weights and edge-aware constraints. However, these filters have limited local perception capabilities and are highly sensitive to the regularization parameter. As the regularization parameter increases, halo artifacts become more severe. Effective guided image filtering (EGIF) [29] incorporates the average of local variances of all pixels into the cost function, accurately preserving edges. This approach is more robust to the regularization parameter and significantly reduces halo artifacts. Therefore, we employ EGIF for illumination estimation.

3 Method

Fig. 2 shows the framework of the proposed method for local content-aware enhancement for low-light Images with non-uniform illumination. The input image P is converted from the RGB to the HSV color model. This method enhances only the Value (brightness) channel V. First, multi-scale effective guided image filtering (MS-EGIF) estimates the illumination component V_I from the Value channel image V. Then, according to the Retinex theory model, the reflectance component V_R is obtained. Next, adaptive gamma correction (AGC) and contrast limited adaptive histogram equalization (CLAHE) are used to adjust the brightness and contrast of the illumination component. Next, EGIF is applied to denoise the reflectance component (E-Denoise). Moreover, the multi-scale detail boosting (MDB) method is applied to enhance the texture details of the denoised reflectance component. Finally, the enhanced illumination component V_{IGH} and the reflectance component V_{RDM} are combined to obtain the enhanced brightness channel image V_E. The linear color restoration (LCR) method is then used to convert the enhanced image back to the original RGB color model, resulting in the final enhanced color image P_E.

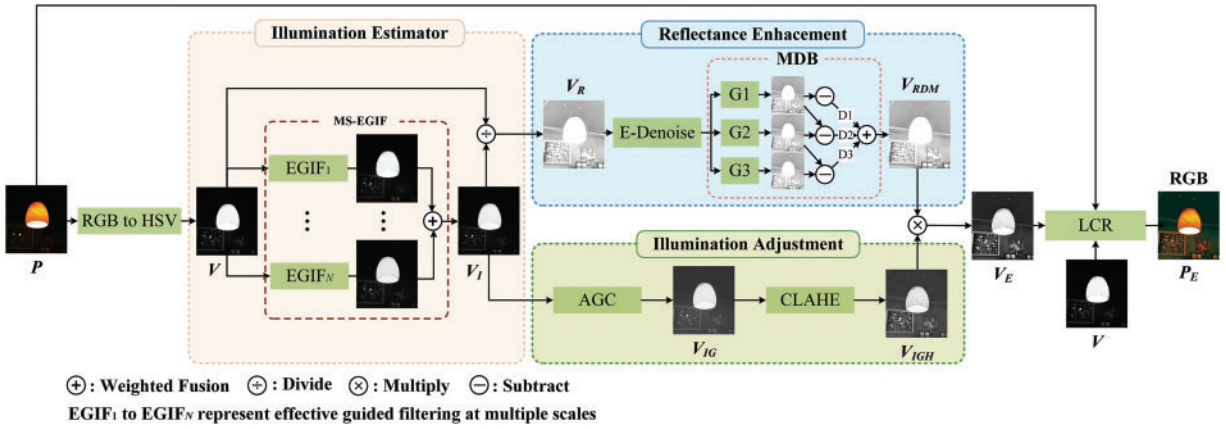

Figure 2: Framework of local content-aware enhancement for low-light Images with non-uniform illumination

3.1 Illumination Estimation

We introduce the MS-EGIF method for illumination estimation. This method enhances the accuracy of illumination estimation by utilizing EGIF across multiple scales to capture both local and global illumination variations, achieving superior detail smoothing and edge preservation.

In the MS-EGIF method, multiple appropriate scale parameters are initially selected using a scale-adaptive selection strategy. Based on these scale parameters, illumination estimation is subsequently conducted using effective guided image filtering. Finally, the illumination components estimated at different scales are weighted and averaged to derive the final illumination component V_I, as shown in Eq. (4).

$$V_I(x,y) = \sum_{i=1}^{N} \alpha \cdot EGIF_i(V(x,y), V(x,y), r_i, \varepsilon) \tag{4}$$

where $EGIF_i()$ represents the EGIF at the i-th scale. Both the guide image and input image use the Value channel image V. r_i denotes the scale parameter, which specifies the filter window size. ε is the regularization parameter set to 0.1. N represents the number of scales. In multi-scale image filtering methods, the number of scales N can be adjusted based on the specific characteristics of the image. However, setting N too high can lead to increased computational costs. As a result, we refer to various multi-scale methods [7,30] and set

the parameter N in MS-EGIF to 3 in the experiments of our method. α represents the weighting coefficient for each scale and is set to $1/N$.

The scale-adaptive selection strategy dynamically adjusts the scale parameters to accommodate images of different sizes, thereby enhancing the perceptual accuracy of the illumination estimation method. As indicated by Eq. (5), smaller images' scale parameters are relatively minor, which helps avoid excessive smoothing while preserving crucial edge information. Conversely, larger images yield larger scale parameters, capturing a broader range of illumination variations while ensuring smooth detail processing. This approach overcomes the limitations of fixed scale parameters by balancing edge preservation with detail smoothing across images of varying sizes, thereby improving the accuracy of illumination estimation.

$$r_1 = \left\lfloor \frac{\min(m,n)}{2^N} \right\rfloor, \quad r_N = \left\lfloor \frac{\max(m,n)}{2} \right\rfloor, \quad r_i = \left\lfloor r_1 + (i-1) \cdot \frac{r_N - r_1}{N-1} \right\rfloor \qquad (i = 2, \ldots, N-1) \tag{5}$$

The EGIF used in the MS-EGIF method is an outstanding edge-preserving smoothing filter. EGIF uses the average of local variances of all pixels as edge-aware weights Γ in Eq. (6), incorporating them into the GIF cost loss function in Eq. (3) to adaptively adjust the regularization parameters ε, as shown in Eq. (7). Γ enhances the filter's ability to detect edges. This leads to more accurate illumination estimation.

$$\Gamma = \overline{\sigma}^2 = \frac{1}{N} \sum_{k=1}^{N} \sigma_k^2 \tag{6}$$

$$E(a_k, b_k) = \sum_{i \in \omega_k} \left[(a_k V_i + b_k - V_i)^2 + \varepsilon \Gamma a_k^2 \right] \tag{7}$$

where σ_k^2 is the local variance of guided image V in ω_k. The partial derivative of the cost loss function is set to zero to calculate the linear constant coefficient (a_k, b_k). Since both the input image and guided image are the Value channel image V, the simplified linear constant coefficients (a_k, b_k) as shown in Eqs. (8) and (9).

$$a_k = \frac{\frac{1}{|\omega|} \sum_{i \in \omega_k} V_i V_i - \mu_k \overline{V}_k}{\sigma_k^2 + \varepsilon \Gamma} = \frac{\sigma_k^2}{\sigma_k^2 + \varepsilon \Gamma} = \frac{1}{1 + \varepsilon \frac{\Gamma}{\sigma_k^2}} = \frac{1}{1 + \varepsilon \frac{\overline{\sigma}^2}{\sigma_k^2}} \tag{8}$$

$$b_k = (1 - a_k)\mu_k \tag{9}$$

where μ_k and σ_k^2 are the mean and variance of the guide image V in ω_k, $|\omega|$ is number of pixels in ω_k.

According to Eqs. (8) and (9), if pixel k is at an edge, the local variance is greater than the average, making a_k and b_k closer to 1 and 0, respectively, for better edge preservation. If pixel k is in a smooth area, the local variance is less than the average, making a_k and b_k closer to 0 and 1 for better smoothing. EGIF adaptively adjusts the regularization parameters to enhance detail textures and edges. It effectively preserves edges at illumination discontinuities while simultaneously smoothing image details.

Following these steps, the estimated illumination component V_I is accurately obtained, and the reflectance component V_R is then derived using Eq. (1).

3.2 Illumination Adjustment

After obtaining the illumination component, our method designs adaptive illumination adjustment. It adjusts enhancement magnitude based on pixel brightness values for precise illumination adjustment. First, the brightness of low-light regions is enhanced through AGC, improving the overall visibility of these areas.

However, it may not be sufficient to recover local details. The image's local contrast is further enhanced using CLAHE, particularly in low-light regions, making the image details clearer.

The adaptive gamma correction function adjusts the gamma correction parameter adaptively based on the value of each pixel in the illumination component image. It corrects the local brightness of the image pixel by pixel to achieve varying degrees of enhancement in dark and bright regions, as shown in Eqs. (10) and (11).

$$V_{IG}(x, y) = V_I(x, y)^{\gamma} \tag{10}$$

$$\gamma = a \cdot V_I(x, y) + b \tag{11}$$

where γ is the correction parameter that determines the enhancement magnitude of each pixel's brightness. The constants a and b range from 0 to 1. Experimental results indicate that the brightness correction is optimized when a and b are set to 0.8 and 0.4, respectively.

Fig. 3 shows the AGC designed in this study (red curve), the standard gamma correction function ($\gamma = 0.3$, $\gamma = 0.5$, $\gamma = 0.8$), and the adaptive gamma correction function curves designed by Shin et al. [31], where our method is indicated in red. The magnified red box area shows that our method significantly suppresses high-brightness areas while enhancing the brightness of dark regions, effectively preventing over-enhancement in bright regions.

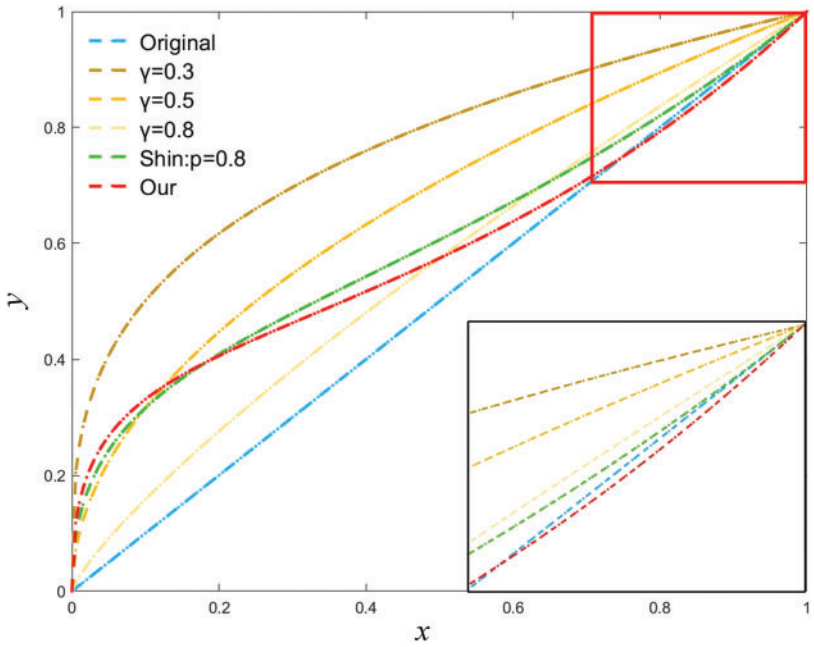

Figure 3: The different gamma correction function curves. The horizontal axis x is the input grayscale value, and the vertical axis y is the output grayscale value

Subsequently, the adjusted illumination component V_{IG} is optimized using CLAHE to enhance the contrast. This process results in the final enhanced illumination component V_{IGH}, as shown in Eq. (12). CLAHE can adaptively adjust the contrast enhancement levels in different regions, enabling better restoration of local image details.

$$V_{IGH}(x, y) = CLAHE(V_{IG}(x, y)) \tag{12}$$

3.3 Reflectance Enhancement

Classical Retinex-based enhancement methods do not consider noise, leading to noise amplification. Direct denoising causes detail loss. We propose an effective reflectance component adjustment method that considers both noise and details, resulting in a reflectance component with reduced noise and clear details.

First, EGIF is used to denoise the reflectance component (E-Denoise), as shown in Eq. (13). EGIF effectively senses noise and textures. It retains as much edge and texture information as possible during denoising.

$$V_{RD}(x,y) = EGIF(V_R(x,y)) \tag{13}$$

A multi-scale local detail enhancement method (MDB) [32] is applied to the denoised reflectance component V_{RD} to make the local details and textures clearer and richer. First, the denoised reflectance component V_{RD} is filtered with three different scale Gaussian kernels to obtain blurred images of varying degrees V_{RDGi}, as shown in Eq. (14).

$$V_{RDGi} = G_{\delta_i} * V_{RD} \tag{14}$$

where G_{δ_i} represents Gaussian kernels of different scales, and the radius of the Gaussian kernel is 3. The standard deviations are $\delta_1 = 1$, $\delta_2 = 2$ and $\delta_3 = 4$, respectively.

Images V_{RDG1}, V_{RDG2} and V_{RDG3} with different blurriness degrees from Eq. (14) extract detail layers D_i assigned weight coefficients h_i, and fused into a detailed image. Adding the detailed image to the denoised reflectance component V_{RD} yields the final denoised and detail-enhanced reflectance component V_{RDM}. The process is shown in Eqs. (15) and (16), where $h_1 = 0.5$, $h_2 = 0.5$ and $h_3 = 0.25$.

$$D_1 = V_{RD} - V_{RDG1}, \quad D_2 = V_{RDG1} - V_{RDG2}, \quad D_3 = V_{RDG2} - V_{RDG3} \tag{15}$$

$$V_{RDM} = V_{RD} + \left[1 - h_1 \times \mathrm{sgn}(D_1)\right] \times D_1 + h_2 \times D_2 + h_3 \times D_3 \tag{16}$$

Finally, the enhanced illumination component V_{IGH} with improved brightness and contrast is fused with the denoised and detail-enhanced reflectance component V_{RDM} to obtain the enhanced value channel image V_E, as shown in Eq. (17).

$$V_E = V_{IGH} \cdot V_{RDM} \tag{17}$$

The enhanced value channel image V_E obtained from the above steps needs to be converted into the final enhanced RGB image P_E. We use an efficient linear color restoration method (LCR) [33] for this conversion, effectively avoiding color distortion.

4 Experiments and Discussion

4.1 Data and Methods

This section validates the effectiveness of the proposed method by comparing it with various existing low-light image enhancement methods. These include traditional methods such as MSRCR [7], MF [34], SRLIE [23], Hong's method [35], and Frequency [36], as well as deep learning methods like Retinex-Net [11], URetinex-Net [13], Retinexformer [25], global structure-aware diffusion (GSAD) [37], and double domain guided network (DDNet) [38]. The code and results for the comparison methods were obtained from the original authors' websites. Default parameters specified in their articles were employed in the experiments. All experiments were conducted using the following setup: Intel Core i7 CPU @ 2.40 GHz, 16 GB RAM, Windows 11 × 64 operating system, and Matlab R2020a experimental platform.

To ensure data diversity, this study utilized images from six low-light image datasets for subjective and objective evaluations. These datasets include DICM [39], LIME [40], MEF [41], NPE [9], VV[1] and LOL [11]. The DICM dataset contains 69 images, 44 captured under low-light conditions. The LIME dataset includes 10 low-light images spanning various scenes. The MEF dataset comprises 9 indoor and 8 outdoor low-light images. The NPE dataset includes 85 low-light images captured under diverse weather and lighting conditions. The VV dataset comprises 24 real multi-exposure images at various resolutions, featuring indoor and outdoor scenes with people and natural landscapes. The LOL dataset contains 500 pairs of low-light and normal-light images. These datasets encompass various lighting conditions, including indoor objects and decor, outdoor buildings, and natural landscapes. Additionally, we evaluated our method's and other methods' average objective metrics and time performance on the DICM, LIME, and MEF datasets.

4.2 Subjective Evaluation

Figs. 4–8 illustrate the enhancement results of our method and other methods for uniform and non-uniform low-illumination color images. Figs. 4 and 7 display the enhancement results of images with uniform and non-uniform illumination, respectively. Fig. 8 displays the local details within the red-boxed regions of the images shown in Fig. 7. Figs. 5 and 6 show the enhancement outcomes of the non-uniform illumination images Candle and Cadik, along with detailed comparisons of local regions.

Figure 4: The enhanced results of different methods in images with uniform low illumination

[1] https://sites.google.com/site/vonikakis/datasets, accessed on 01 November 2024.

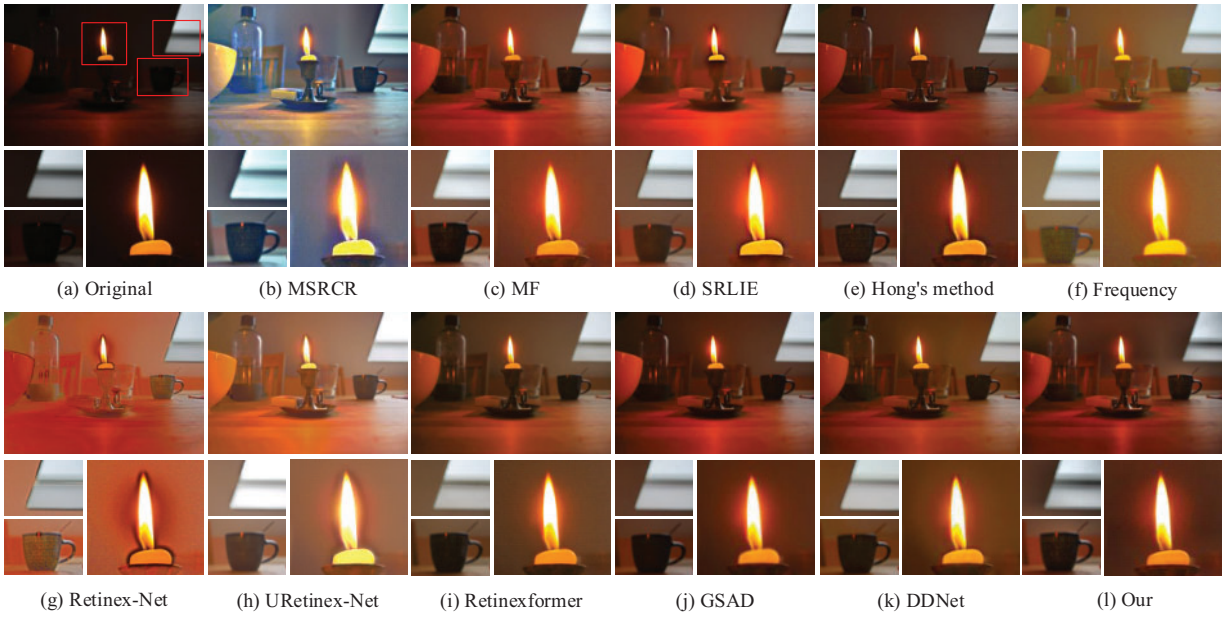

Figure 5: The detailed enhanced results of different methods in Candle

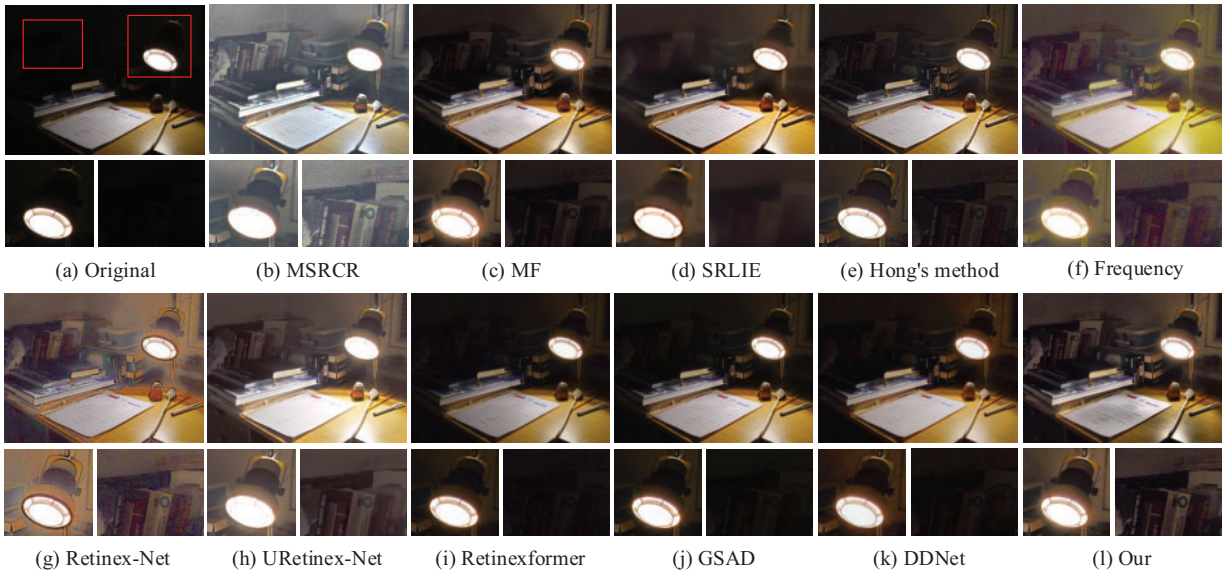

Figure 6: The detailed enhanced results of different methods in Cadik

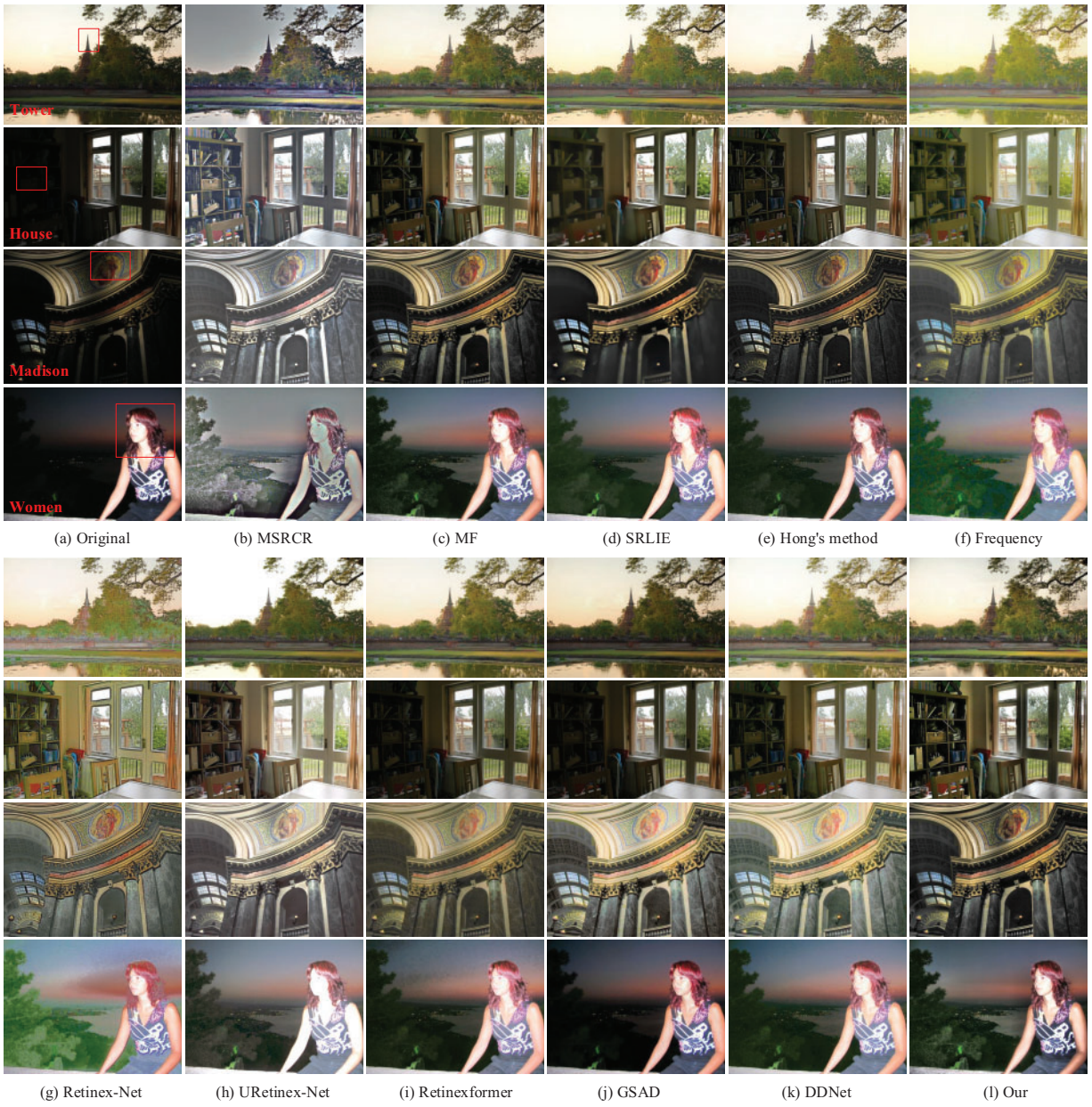

Figure 7: The enhanced results of different methods in images with non-uniform low illumination

Figure 8: The detailed enhanced results of different methods in images with non-uniform low illumination: (a) Original images, (b) MSRCR, (c) MF, (d) SRLIE, (e) Hong's method, (f) Frequency, (g) Retinex-Net, (h) URetinex-Net, (i) Retinexformer, (j) GSAD, (k) DDNet, (l) Ours

As shown in Fig. 4, these methods effectively enhance the brightness of images with uniform low-light conditions, revealing more detailed information. Among them, MSRCR, Frequency, Retinex-Net, and URetinex-Net exhibit the most significant improvements in brightness. However, each of these methods introduces varying degrees of color distortion. Although SRLIE effectively reduces noise, it blurs image details, as shown in Fig. 4d. In comparison, MF, Hong's method, and the proposed method achieve satisfactory enhancement effects. However, MF produces slightly lower image sharpness than the proposed method, as seen in Fig. 4c. The Hong's method and GSAD show insufficient brightness enhancement for images in extremely low-light conditions, as shown in Fig. 4e,j. Retinexformer and DDNet improve brightness in uniformly low-light images and maintain natural color in the enhanced images. However, DDNet suffers from reduced image sharpness, as shown in Fig. 4k.

As shown in Figs. 5–8, the MSRCR, Retinex-Net, and URetinex-Net methods effectively enhance brightness in the dark regions of images with non-uniform illumination. However, MSRCR and Retinex-Net exhibit severe halo artifacts, color distortion, and noise amplification. The URetinex-Net method suffers from substantial detail loss in the bright regions and presents low contrast, giving the image an overall washed-out appearance. In contrast, MF, SRLIE, Hong's method, Frequency, DDNet, and the proposed method manage Non-Uniform Illumination effectively, enhancing brightness in dark regions without over-enhancing bright areas. Despite this, these methods still have some limitations. For instance, the SRLIE and Hong's method fail to effectively address edge artifacts, with halos still visible around the candle base in Fig. 5d,e. SRLIE results in significant details blurring in dark regions, as shown in Fig. 7d. The Frequency produces blurred edges and unnatural color in enhanced images, as shown in Fig. 7f. The detail sharpness of images enhanced by DDNet is slightly inferior to that achieved by the proposed method, as shown in Fig. 7k. Additionally, Retinexformer and GSAD show limited brightness enhancement in dark regions, which leads to obscured details, as illustrated by the Cadik image in Fig. 6i,j.

Overall, our method demonstrates significant advantages in handling images with non-uniform illumination. The images enhanced by our method demonstrate no significant halo artifacts in areas with abrupt changes in illumination, and the colors are rendered more vividly and authentically. Both dark and bright regions are well-enhanced. For example, the inner frame of the lamp in the Cadik image in Fig. 6l and the clouds in the Tower image in Fig. 7l are well-defined. Additionally, our method preserves precise details in enhanced images, as seen in the books in the Cadik image in Fig. 6l and the portrait in the Madison

image in Fig. 7l. However, compared to URetinex-Net and Retinexformer, our algorithm still has room for improvement in noise reduction in extremely dark regions of non-uniform illumination images, as illustrated by the magnified details in the Cadik image in Fig. 6l and the wall in the House image in Fig. 7l.

4.3 Objective Evaluation

To comprehensively and objectively evaluate the enhancement effects of the proposed method and its comparison methods, we will use the following seven objective metrics to measure the quality of the enhanced images from detail richness, sharpness, color, contrast, and naturalness perspectives. (1) Information entropy (IE) is employed to assess the richness of image information. A greater value of IE indicates a richer abundance of detail. (2) The energy of the gradient (EOG) is utilized to evaluate image sharpness. A higher value of EOG reflects improved image sharpness. (3) ΔH measures the degree of hue change before and after processing. A lower color variation rate signifies better color fidelity before and after processing. (4) Contrast enhancement-based image quality (CEIQ) [42] is a no-reference image quality assessment metric designed to measure image contrast using features such as structural similarity, histogram-based entropy, and cross-entropy. A greater value of CEIQ indicates a better-quality image. (5) Entropy-based no-reference image quality assessment (ENIQA) [43] is a high-performance general-purpose no-reference (NR) image quality assessment (IQA) method based on image entropy. It effectively evaluates the quality of various distorted images by leveraging features from both spatial and frequency domains, including mutual information and entropy. (6) The blind/referenceless image spatial quality evaluator (BRISQUE) [44] is a no-reference image quality assessment model based on natural scene statistics that quantifies the loss of naturalness in an image due to distortions by analyzing locally normalized luminance coefficients in the spatial domain. This model effectively assesses the overall quality of an image. (7) The natural image quality evaluator (NIQE) [45] is a blind image quality assessment model designed to predict the quality of distorted images by analyzing measurable deviations from statistical regularities observed in natural images. ENIQA, BRISQUE, and NIQE assess image naturalness from different perspectives, with lower values indicating higher and more natural quality.

Table 1 presents the objective evaluation metrics for selected images used in the subjective assessment of this study. Tables 2 and 3 display the average NIQE, BRISQUE, and CEIQ values, along with the average time performance, for various methods applied to images from the DICM, MEF, and LIME datasets. The best values are highlighted in red, and the second-best values are highlighted in blue. Subjective evaluations reveal that images enhanced by MSRCR exhibit severe distortion, adversely affecting visual perception. In contrast, the other comparative methods, including ours, show favorable enhancement results. To further evaluate the strengths and weaknesses of these methods, various objective metrics are used to compare image detail richness, clarity, color, contrast, and naturalness.

Table 1: Objective evaluation metrics of different enhancement methods for low illumination images

Method		Indicator						
		IE↑	EOG($\times 10^{11}$) ↑	ΔH ↓	**CEIQ↑**	**ENIQA↓**	**BRISQUE↓**	**NIQE↓**
DICM-Factory	MF	7.2620	0.5572	0.0244	3.2908	0.1069	21.6814	2.3726
	SRLIE	6.9608	0.4477	0.0643	3.3177	0.2999	38.2658	3.8697
	Hong's method	7.1184	1.3862	0.0256	3.1925	0.0740	21.7161	2.3699

(Continued)

Table 1 (continued)

Method		Indicator						
		IE↑	EOG($\times 10^{11}$) ↑	ΔH ↓	CEIQ↑	ENIQA↓	BRISQUE↓	NIQE↓
	Frequency	7.0201	0.0845	0.1831	3.2301	0.1192	29.0286	2.9417
	Retinex-Net	7.0449	1.6463	0.1507	3.2325	0.1783	39.5511	4.8757
	URetinex-Net	7.4329	0.5788	0.0898	3.4646	0.1223	23.5859	3.1239
	Retinexformer	6.6902	0.2002	0.1018	2.8269	0.0576	21.7077	3.6692
	GSAD	7.6976	0.1930	0.4122	3.2917	0.1024	9.9809	2.6840
	DDNet	6.6418	0.1724	0.1244	2.7505	0.0921	19.3646	3.7576
	our method	7.3970	0.9864	0.0198	3.3951	0.0641	19.3265	2.3323
LOL-Cupboard	MF	6.8430	0.1233	0.0408	3.1334	0.0305	15.5981	4.1473
	SRLIE	6.0061	0.0037	0.0634	2.8050	0.3780	58.1363	7.7840
	Hong's method	6.2383	0.0551	0.0392	2.8346	0.0605	16.7735	3.9147
	Frequency	6.0134	0.0021	0.0264	2.7264	0.2550	28.9116	8.1477
	Retinex-Net	6.5363	0.5904	0.0543	2.9100	0.3651	44.9004	8.7300
	URetinex-Net	6.6950	0.3310	0.2437	3.1235	0.0953	25.2134	6.4224
	Retinexformer	7.1413	0.0312	0.1881	3.2959	0.1533	31.9828	4.8168
	GSAD	5.9945	0.0113	0.1630	2.3215	0.0983	22.1940	5.2969
	DDNet	6.2426	0.0164	0.3451	3.3641	0.1176	15.8851	4.8093
	our method	6.9138	0.0650	0.0367	3.1033	0.0582	15.2892	4.1135
NPE-Tower	MF	7.3624	2.3743	0.0445	3.4096	0.0290	27.3605	2.8620
	SRLIE	6.9999	1.0867	0.0176	3.2222	0.2163	33.6940	3.1045
	Hong's method	7.1178	23.6637	0.0207	3.2961	0.0441	38.8743	2.8364
	Frequency	6.6815	0.2316	0.0093	2.9753	0.1525	19.9741	2.9733
	Retinex-Net	7.2632	18.2832	0.0378	3.3129	0.0513	28.0227	5.1893
	URetinex-Net	5.9693	16.0408	0.2588	3.1779	0.0145	65.3364	4.9518
	Retinexformer	7.0819	3.1248	0.0482	3.2488	0.0198	5.0422	3.1106
	GSAD	6.7310	0.7393	0.9840	2.7727	0.0101	6.3052	3.5687
	DDNet	7.2359	2.1230	0.0483	3.2654	0.0060	8.7927	2.6781
	our method	7.5681	8.0677	0.0366	3.5258	0.0354	13.8076	2.5644
MEF-House	MF	7.7272	0.3255	0.0103	3.5250	0.1288	24.1788	3.4237
	SRLIE	7.5575	0.2332	0.0892	3.4531	0.2163	37.7641	4.4593
	Hong's method	7.6257	0.6478	0.0062	3.4535	0.1004	27.6591	3.2346
	Frequency	7.7188	0.0186	0.0468	3.5679	0.1215	32.7833	4.2532
	Retinex-Net	7.5845	0.6491	0.0325	3.4910	0.0401	30.6925	5.9544

(Continued)

Table 1 (continued)

Method		IE↑	EOG($\times 10^{11}$) ↑	ΔH ↓	CEIQ↑	ENIQA↓	BRISQUE↓	NIQE↓
	URetinex-Net	7.7084	0.1668	0.1076	3.6674	0.0351	35.3075	4.3369
	Retinexformer	7.3753	0.0891	0.0650	3.1553	0.0469	22.2122	3.9231
	GSAD	7.3440	0.0504	0.1315	3.2376	0.0752	16.4777	3.2783
	DDNet	7.7047	0.0819	0.0414	3.5384	0.0636	22.2361	3.6122
	our method	7.6922	0.7538	0.0170	3.5837	0.0322	23.6186	3.3462
MEF-Madison	MF	7.3658	1.9665	0.0747	3.2408	0.0707	14.3839	2.2622
	SRLIE	7.1308	0.8459	0.0231	3.1279	0.1901	37.2088	4.0156
	Hong's method	7.1980	2.4612	0.0735	3.1117	0.0361	17.5521	2.8149
	Frequency	7.0900	0.0675	0.0335	3.1998	0.1390	22.3889	3.0308
	Retinex-Net	7.3145	2.0984	0.0988	3.3633	0.0525	35.3800	4.5882
	URetinex-Net	7.3700	0.7494	0.6951	3.3713	0.0287	16.0342	2.5939
	Retinexformer	7.0607	0.1128	0.3260	3.1190	0.0599	14.5840	2.6023
	GSAD	6.1413	0.7216	0.2222	2.3309	0.0694	20.5123	2.7792
	DDNet	7.3935	0.3865	0.0742	3.3698	0.0673	13.3987	2.7301
	our method	7.4676	0.8111	0.0872	3.3891	0.0999	9.1946	2.4236

Table 2: Quantitative comparison of the DICM, MEF, LIME datasets using NIQE, BRISQUE, CEIQ indicators

Method	DICM			MEF			LIME		
	NIQE↓	BRISQUE↓	CEIQ↑	NIQE↓	BRISQUE↓	CEIQ↑	NIQE↓	BRISQUE↓	CEIQ↑
MF	3.6942	23.8183	3.2458	3.5713	17.7639	3.1819	4.1522	20.9914	3.1867
SRLIE	6.4623	47.0398	3.1759	7.6614	55.0069	3.2082	4.5407	32.7560	3.1564
Hong's method	3.6626	26.4078	3.1997	3.1225	22.9110	3.1225	4.1411	23.3331	3.0600
Frequency	4.4230	31.0492	3.0966	4.1693	21.4112	3.1451	4.8479	21.8146	3.1590
Retinex-Net	4.4073	30.9511	3.1469	4.2428	20.0950	3.2008	4.7311	27.0441	3.2193
URetinex-Net	3.9805	20.5915	3.3144	3.6099	19.7734	3.3781	4.5735	24.9238	3.3301
Retinexforme	3.9525	15.1985	3.0898	3.6334	15.1867	3.0127	4.5347	21.0497	3.1759
GSAD	4.2973	20.4079	3.0761	3.8730	18.3098	3.0394	4.3074	18.5721	3.0697
DDNet	3.9047	19.2697	3.1489	3.4659	15.4604	3.1888	4.1342	16.3115	3.1303
Our	3.5919	23.0790	3.3582	3.0893	17.3364	3.2565	4.1288	20.8058	3.1864

Table 3: Comparison of the average processing time of different algorithms in the DICM, MEF, LIME dataset (unit: second)

	Method										
Datasets	**MSRCR**	**MF**	**SRLIE**	**Hong's method**	**Frequency**	**Retinex-Net**	**URetinex-Net**	**Retinexformer**	**GSAD**	**DDNet**	**Ours**
LIME	0.4033	0.1562	0.2374	0.0760	8.1072	0.6471	0.0428	0.1704	1.2134	0.1275	0.1485
MEF	0.2730	0.1891	0.1369	0.0540	2.8169	0.2781	0.0261	0.1263	0.5790	0.1101	0.0960
DICM	0.4177	0.1638	0.1934	0.0963	6.3938	0.1675	0.0489	0.1490	1.0143	0.1343	0.1857

As shown in Table 1, images processed by our method under various lighting conditions achieved the best or second-best results across multiple metrics. This indicates that our approach performs well regarding image detail richness, sharpness, color fidelity, contrast, and naturalness under diverse lighting conditions, consistent with subjective evaluations. Specifically, Retinex-Net and Frequency methods lead to color distortion in enhanced images, reflected in their higher ΔH values. SRLIE generates blurry images, resulting in lower performance across several metrics, including low EOG and high ENIQA values. URetinex-Net tends to excessively enhance bright regions when processing images with non-uniform lighting, yielding less natural images and higher NIQE values. GSAD demonstrates limited brightness enhancement capabilities, and the loss of image details results in a lower IE value. Both MF and Hong's method yield good overall enhancement results. However, their CEIQ and BRISQUE values are slightly lower than our method, indicating that contrast and overall quality are marginally inferior. DDNet and Retinexformer exhibit favorable results on naturalness-related metrics. However, their detail sharpness needs to be improved, with EOG values slightly lower than those obtained by our method.

As illustrated in Table 2, our method consistently achieves the best NIQE scores across three datasets and obtains optimal or near-optimal values in the BRISQUE and CEIQ metrics. This indicates that our method reliably enhances low-light images under various illumination conditions and across diverse scenes. Although our method does not achieve the highest score for every metric on each dataset, it provides the best overall enhancement effect with better robustness.

Table 3 presents the average processing time for enhancing low-light images in the DICM, MEF, and NPE datasets using the algorithms discussed. As shown in Table 3, Hong's method and URetinex-Net demonstrate shorter processing times, whereas MSRCR, Frequency, Retinex-Net, and GSAD require longer processing times. The runtime of MF, Retinexformer, DDNet, and our method is comparable. Considering both subjective and objective evaluations, as well as the time efficiency of each algorithm, our method achieves the best overall performance.

4.4 Ablation Experiment

To verify the necessity of each processing module used in our method, we conducted an ablation experiment. The experiments include: (a) without adaptive gamma correction (w/o AGC), (b) without contrast limited adaptive histogram equalization (w/o CLAHE), (c) without EGIF denoising (w/o ED), (d) without multi-scale detail boosting (w/o MDB), and (e) the complete proposed method. The ablation study design is shown in Table 4. Due to space constraints, only two images, Cadik and Desk, from different scenes are presented for the ablation study. The final experimental results are displayed in Figs. 9 and 10.

Table 4: Ablation experiment design and objective evaluation results

	AGC	CLAHE	E-Denoise	MDB	Cadik/Desk ablation study quality evaluation		
					NIQE↓	BRISQUE↓	CEIQ↑
(a)w/o AGC	×	✓	✓	✓	4.5701/2.7518	18.6531/22.7059	2.5907/2.9207
(b)w/o CLAHE	✓	×	✓	✓	3.7433/2.8281	20.7335/21.3895	3.1371/3.0971
(c)w/o E-Denoise	✓	✓	×	✓	3.1660/2.4541	18.3308/19.5756	3.2912/3.4418
(d)w/o MDB	✓	✓	✓	×	3.4330/2.5893	20.9889/21.5155	3.2677/3.4095
(e)Our	✓	✓	✓	✓	3.1598/2.4242	18.1817/19.2343	3.2926/3.4427

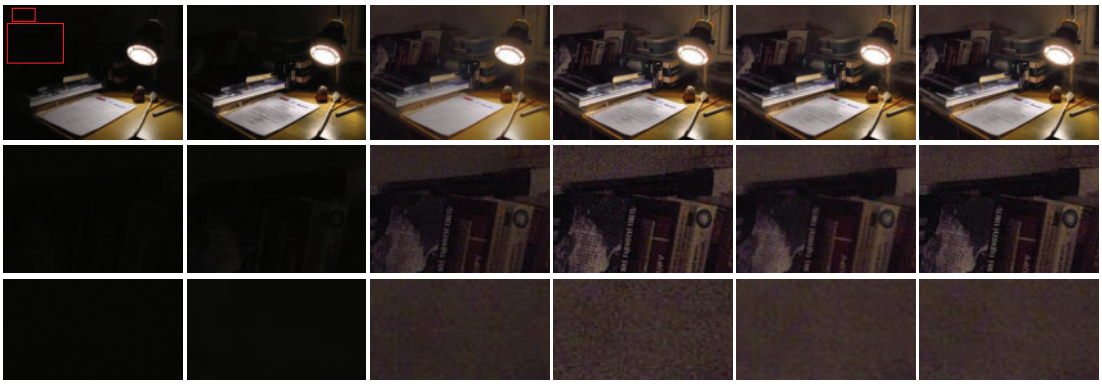

(a) Original (b)w/o AGC (c) w/o CLAHE (d) w/o E-Denoise (e) w/o MDB (f) Our

Figure 9: Ablation experiment results in Cadik image

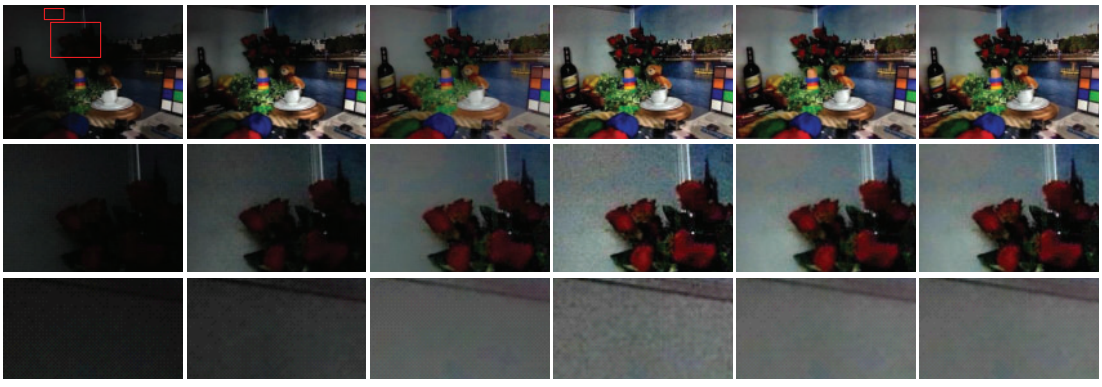

(a) Original (b)w/o AGC (c) w/o CLAHE (d) w/o E-Denoise (e) w/o MDB (f) Our

Figure 10: Ablation experiment results in Desk image

Figs. 9 and 10 show the results of the ablation study for each design scheme, leading to the following conclusions: (a) Without AGC, the overall brightness of the image is low, and the enhancement of dark areas is insufficient, as seen in the books against the wall in Fig. 9a. (b) Without CLAHE, the image

brightness is significantly enhanced, but the recovery of local details is insufficient. (c) Without E-Denoise, the image details are richer, and edge textures are clearer. However, the noise is significantly amplified, and the image looks unnatural. (e.g., the wall sections in Fig. 9c and Fig. 10c). (d) Without MDB, the noise is effectively filtered out, but detailed texture information is blurred, resulting in a less clear image. (e) Our method, which includes complete processing modules, performs better in brightness, contrast enhancement, denoising, and detail enhancement. Additionally, Table 4 presents the objective evaluation metrics for all images in Figs. 9 and 10, where our method achieves the best values in multiple metrics, outperforming the other compared images.

4.5 Parameter Analysis Experiment

In this section, we evaluate the relevant parameters in the paper, specifically the regularization parameter ε in Eq. (7) and the parameters a and b in Eq. (11). To facilitate a more intuitive analysis of the impact of parameter variations on image enhancement effects, this section directly displays the values of relevant objective evaluation metrics below the corresponding images.

First, we assess the regularization parameter ε in Eq. (7) by setting it to the values in the set $(0.01, 0.1, 1)$ and observing the corresponding results. The IE and BRISQUE metrics are used to evaluate these outcomes. Fig. 11 illustrates that the estimated illumination component becomes smoother as the regularization parameter ε increases. However, when ε is set to 1, the image exhibits edge blurring. Conversely, smaller ε values enhance the image's brightness and clarity but also significantly increase noise levels. Therefore, to balance the impact of brightness, clarity, and noise, we select 0.1 as the default parameter. Objective evaluation metrics indicate that variations in the regularization parameter ε have a relatively minor impact on enhancement performance. This is because the EIGF in MS-EGIF designed in our method incorporates edge-aware weights that enable adaptive adjustment of the regularization parameter ε, thereby effectively avoiding poor enhancement results due to improper parameter settings.

In Eq. (11), the AGC function determines the gamma correction parameter primarily based on the parameters a and b, along with the pixel value at each point. To systematically explore the effects of these parameters, we selected a series of values for a and b: $(0.2, 0.4, 0.6, 0.8, 1)$ and conducted comprehensive experimental evaluations on each combination. Fig. 12 presents the detailed impact of these parameter combinations on the experimental results. BRISQUE and CEIQ metrics were employed to assess each result.

As shown in Fig. 12, parameter a minimizes impact on the overall enhancement results. When b is fixed, the decreasing parameter a results in a slight improvement in image contrast. In contrast, parameter b has a more significant influence on image brightness. With a fixed, as b decreases, the image brightness and contrast gradually increase. The BRISQUE score decreases rapidly, while the CEIQ score gradually increases, indicating a significant improvement in overall image quality. When b is reduced to below 0.4, the BRISQUE value stabilizes. However, if b becomes too low, the color naturalness deteriorates. Therefore, our experiments set $a = 0.8$ and $b = 0.4$ as the default parameters to achieve a balanced overall enhancement effect.

5 Conclusion

Despite the exceptional performance of deep learning in image enhancement, traditional methods retain their prevalence in resource-limited scenarios, such as embedded devices, industrial inspection, and mobile processing. We propose a local content-aware enhancement method for low-light images with non-uniform illumination. MS-EGIF is used for localized illumination estimation, improving the accuracy of illumination estimation. It can effectively solve the halo artifacts often appearing in enhanced non-uniform illumination images. To avoid over-enhancement of bright regions, an AGC function is designed to enhance

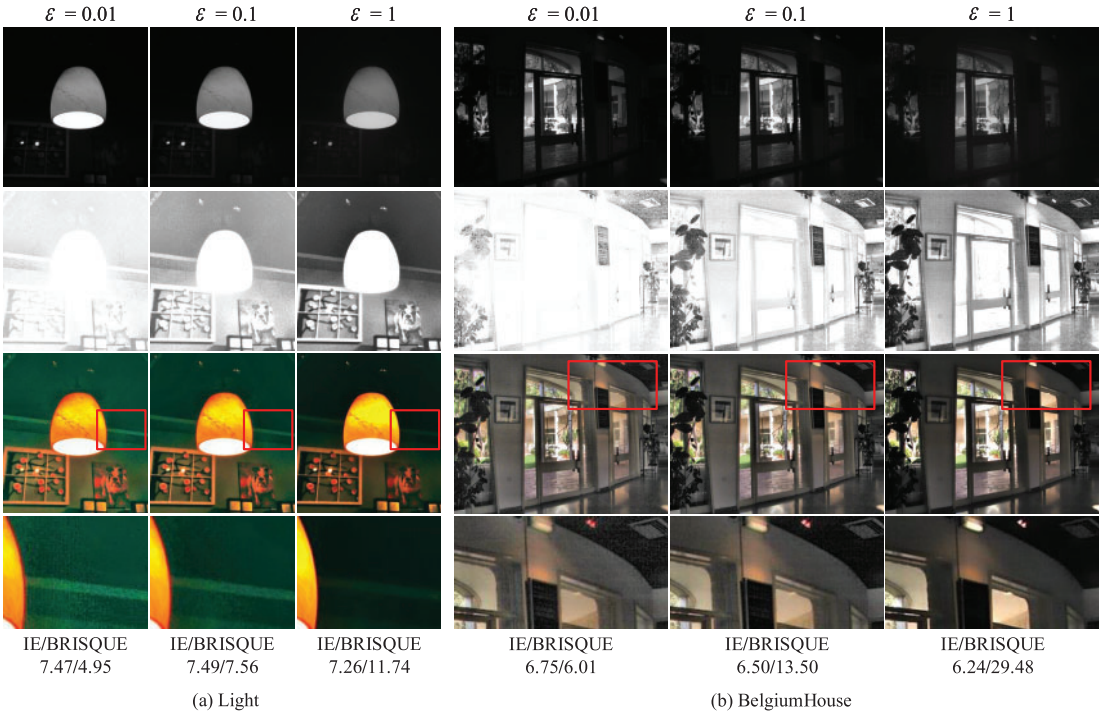

Figure 11: The enhanced results of different regularization parameter values ε in Light and BelgiumHouse images

the brightness of dark areas while effectively suppressing bright regions. EGIF and MDB methods adjust the reflectance component. This ensures noise reduction while preserving image details.

Experimental results show that the proposed method can efficiently enhance images captured under uniform illumination. Compared to existing methods, the resulting images show significant improvements in addressing halo artifacts and over-enhancement in bright regions. Additionally, the images exhibit natural colors and display more prosperous, more precise details. Although the method achieves satisfactory enhancement results, it still exhibits limitations in denoising in low-light regions when dealing with images with extremely non-uniform illumination. Resolving this issue will be part of our future work.

Acknowledgement: None.

Funding Statement: The authors received no specific funding for this study.

Author Contributions: The authors confirm contribution to the paper as follows: study conception and design: Qi Mu, Zhanli Li; data collection: Yuanjie Guo, Xinyue Wang; analysis and interpretation of results: Qi Mu, Yuanjie Guo, Xiangfu Ge; draft manuscript preparation: Qi Mu, Yuanjie Guo. All authors reviewed the results and approved the final version of the manuscript.

Availability of Data and Materials: The data and materials used to support the findings of this study are available from the corresponding author upon request.

Ethics Approval: Not applicable.

Conflicts of Interest: The authors declare no conflicts of interest to report regarding the present study.

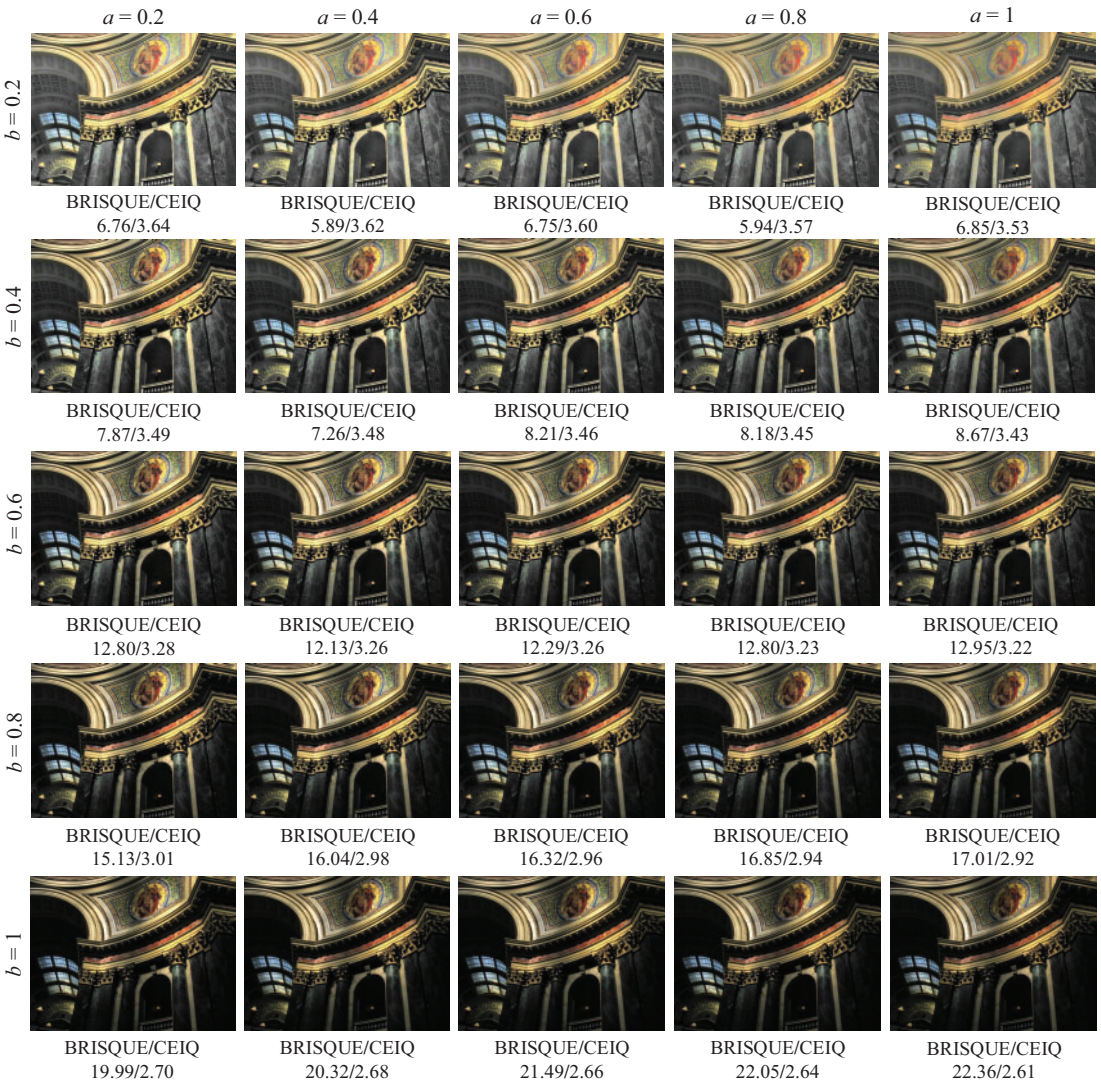

Figure 12: The enhanced results of different parameter values a and b in Madison images

References

1. Li C, Guo C, Han L, Jiang J, Cheng M-M, Gu J, et al. Low-light image and video enhancement using deep learning: a survey. IEEE Trans Pattern Anal Mach Intell. 2022;44(12):9396–416. doi:10.1109/TPAMI.2021.3126387.
2. Liu X, Wu Z, Li A, Vasluianu F-A, Zhang Y, Gu S, et al. Ntire 2024 challenge on low light image enhancement: methods and results. In: Proceedings of the IEEE/CVF Conference on Computer Vision and Pattern Recognition (CVPR); 2024; Seattle, WA, USA: IEEE. p. 6571–94.
3. Land EH. The retinex theory of color vision. Sci Am. 1977;237(6):108–29. doi:10.1038/scientificamerican1277-108.
4. Lin Y-H, Lu Y-C. Low-light enhancement using a plug-and-play retinex model with shrinkage mapping for illumination estimation. IEEE Trans Image Process. 2022;31:4897–908. doi:10.1109/TIP.2022.3189805.
5. Du S, Zhao M, Liu Y, You Z, Shi Z, Li J, et al. Low-light image enhancement and denoising via dual-constrained retinex model. Appl Math Model. 2023;116:1–15. doi:10.1016/j.apm.2022.11.022.
6. Yi X, Xu H, Zhang H, Tang L, Ma J. Diff-Retinex: rethinking low-light image enhancement with a generative diffusion model. In: Proceedings of the IEEE/CVF International Conference on Computer Vision (ICCV); 2023 Oct; Paris, France: IEEE. p. 12302–11.

7. Rahman Z-U, Jobson DJ, Woodell GA. Retinex processing for automatic image enhancement. J Electron Imaging. 2004;13(1):100–10. doi:10.1117/1.1636183.
8. Wang W, Wu X, Yuan X, Gao Z. An experiment-based review of low-light image enhancement methods. IEEE Access. 2020;8:87 884–917. doi:10.1109/ACCESS.2020.2992749.
9. Wang S, Zheng J, Hu H-M, Li B. Naturalness preserved enhancement algorithm for non-uniform illumination images. IEEE Trans Image Process. 2013;22(9):3538–48. doi:10.1109/TIP.2013.2261309.
10. Mu Q, Wang X, Wei Y, Li Z. Low and non-uniform illumination color image enhancement using weighted guided image filtering. Comput Vis Media. 2021;7(4):529–46. doi:10.1007/s41095-021-0232-x.
11. Wei C, Wang W, Yang W, Liu J. Deep retinex decomposition for low-light enhancement. arXiv:1808.04560. 2018.
12. Zhang Y, Zhang J, Guo X. Kindling the darkness: A practical low-light image enhancer. In: Proceedings of the 27th ACM International Conference on Multimedia; 2019; New York, NY, USA: ACM. p. 1632–40.
13. Wu W, Weng J, Zhang P, Wang X, Yang W, Jiang J. Uretinex-Net: retinex-based deep unfolding network for low-light image enhancement. In: Proceedings of the IEEE/CVF Conference on Computer Vision and Pattern Recognition (CVPR); 2022; New Orleans, LA, USA: IEEE. p. 5901–10.
14. Ye J, Qiu C, Zhang Z. A survey on learning-based low-light image and video enhancement. Displays. 2023;81:102614.
15. Jeon JJ, Park JY, Eom IK. Low-light image enhancement using gamma correction prior in mixed color spaces. Pattern Recognit. 2024;146:110001. doi:10.1016/j.patcog.2023.110001.
16. Paul A. Adaptive tri-plateau limit tri-histogram equalization algorithm for digital image enhancement. Vis Comput. 2023;39(1):297–318. doi:10.1007/s00371-021-02330-z.
17. Veluchamy M, Subramani B. Fuzzy dissimilarity color histogram equalization for contrast enhancement and color correction. Appl Soft Comput. 2020;89(1):106077. doi:10.1016/j.asoc.2020.106077.
18. Chang Y, Jung C, Ke P, Song H, Hwang J. Automatic contrast-limited adaptive histogram equalization with dual gamma correction. IEEE Access. 2018;6:11 782–92. doi:10.1109/ACCESS.2018.2797872.
19. Tomasi C, Manduchi R. Bilateral filtering for gray and color images. In: Sixth International Conference on Computer Vision (IEEE Cat. No. 98CH36271); 1998; Bombay, India: IEEE. p. 839–46.
20. He K, Sun J, Tang X. Guided image filtering. IEEE Trans Pattern Anal Mach Intell. 2012;35(6):1397–409. doi:10.1109/TPAMI.2012.213.
21. Xu X, Yu Z. Low-light image enhancement based on retinex theory. In: 2023 IEEE 6th International Conference on Electronic Information and Communication Technology (ICEICT); 2023; Qingdao, China: IEEE. p. 1–6.
22. Fu X, Zeng D, Huang Y, Zhang X-P, Ding X. A weighted variational model for simultaneous reflectance and illumination estimation. In: Proceedings of the IEEE Conference on Computer Vision and Pattern Recognition (CVPR); 2016; Las Vegas, NV, USA: IEEE. p. 2782–90.
23. Li M, Liu J, Yang W, Sun X, Guo Z. Structure-revealing low-light image enhancement via robust retinex model. IEEE Trans Image Process. 2018;27(6):2828–41. doi:10.1109/TIP.2018.2810539.
24. Zhang Y, Guo X, Ma J, Liu W, Zhang J. Beyond brightening low-light images. Int J Comput Vis. 2021;129(4):1013–37. doi:10.1007/s11263-020-01407-x.
25. Cai Y, Bian H, Lin J, Wang H, Timofte R, Zhang Y. Retinexformer: one-stage retinex-based transformer for low-light image enhancement. In: Proceedings of the IEEE/CVF International Conference on Computer Vision (ICCV); 2023; Paris, France: IEEE. p. 12504–13.
26. Yin J, Li H, Du J, He P. Low illumination image retinex enhancement algorithm based on guided filtering. In: 2014 IEEE 3rd International Conference on Cloud Computing and Intelligence Systems; 2014; Shenzhen, China: IEEE. p. 639–44.
27. Li Z, Zheng J, Zhu Z, Yao W, Wu S. Weighted guided image filtering. IEEE Trans Image Process. 2014;24(1):120–9.
28. Kou F, Chen W, Wen C, Li Z. Gradient domain guided image filtering. IEEE Trans Image Process. 2015;24(11):4528–39. doi:10.1109/TIP.2015.2468183.
29. Lu Z, Long B, Li K, Lu F. Effective guided image filtering for contrast enhancement. IEEE Signal Process Lett. 2018;25(10):1585–9. doi:10.1109/LSP.2018.2867896.
30. He Z, Mo H, Xiao Y, Cui G, Wang P, Jia L. Multi-scale fusion for image enhancement in shield tunneling: a combined MSRCR and clahe approach. Meas Sci Technol. 2024;35(5):056112. doi:10.1088/1361-6501/ad25e4.

31. Shin Y, Jeong S, Lee S. Content awareness-based color image enhancement. In: The 18th IEEE International Symposium on Consumer Electronics (ISCE 2014); 2014; Jeju, Republic of Korea: IEEE. p. 1–2.
32. Kim Y, Koh YJ, Lee C, Kim S, Kim C-S. Dark image enhancement based onpairwise target contrast and multi-scale detail boosting. In: 2015 IEEE International Conference on Image Processing (ICIP); 2015; Quebec City, QC, Canada: IEEE. p. 1404–8.
33. Gorai A, Ghosh A. Hue-preserving color image enhancement using particle swarm optimization. In: 2011 IEEE Recent Advances in Intelligent Computational Systems; 2011. p. 563–8.
34. Fu X, Zeng D, Huang Y, Liao Y, Ding X, Paisley J. A fusion-based enhancing method for weakly illuminated images. Signal Process. 2016;129(12):82–96. doi:10.1016/j.sigpro.2016.05.031.
35. Hong Y, Zhu DP, Gong PS. Retinex mine image enhancement algorithm based on tophat weighted guided filtering. J Mine Automat. 2022;48(8):43–9. doi:10.13272/j.issn.1671-251x.2022020029.
36. Zhou M, Leng H, Fang B, Xiang T, Wei X, Jia W. Low-light image enhancement via a frequency-based model with structure and texture decomposition. ACM Transact Multim Comput Communicat Appl. 2023;19(6):1–23. doi:10.1145/3590965.
37. Hou J, Zhu Z, Hou J, Liu H, Zeng H, Yuan H. Global structure-aware diffusion process for low-light image enhancement. In: Proceedings of the 37th International Conference on Neural Information Processing Systems (NIPS '23); 2024; Red Hook, NY, USA: Curran Associates Inc. Vol. 36, p. 79734–47.
38. Qu J, Liu RW, Gao Y, Guo Y, Zhu F, Wang F-Y. Double domain guided real-time low-light image enhancement for ultra-high-definition transportation surveillance. IEEE Trans Intell Transp Syst. 2024;25(8):9550–62. doi:10.1109/TITS.2024.3359755.
39. Lee C, Lee C, Kim C-S. Contrast enhancement based on layered difference representation of 2D histograms. IEEE Trans Image Process. 2013;22(12):5372–84. doi:10.1109/TIP.2013.2284059.
40. Guo X, Li Y, Ling H. Lime: low-light image enhancement via illumination map estimation. IEEE Trans Image Process. 2016;26(2):982–93.
41. Ma K, Zeng K, Wang Z. Perceptual quality assessment for multi-exposure image fusion. IEEE Trans Image Process. 2015;24(11):3345–56. doi:10.1109/TIP.2015.2442920.
42. Yan J, Li J, Fu X. No-reference quality assessment of contrast-distorted images using contrast enhancement. arXiv preprint arXiv:1904.08879. 2019.
43. Chen X, Zhang Q, Lin M, Yang G, He C. No-reference color image quality assessment: from entropy to perceptual quality. EURASIP J Image Video Process. 2019;2019:1–14.
44. Mittal A, Moorthy AK, Bovik AC. No-reference image quality assessment in the spatial domain. IEEE Trans Image Process. 2012;21(12):4695–708. doi:10.1109/TIP.2012.2214050.
45. Mittal A, Soundararajan R, Bovik AC. Making a "completely blind" image quality analyzer. IEEE Signal Process Lett. 2012;20(3):209–12.